Charge Transfer at Hybrid Interfaces: Plasmonics of Aromatic Thiol-Capped Gold Nanoparticles

Claire Goldmann,[†] Rémi Lazzari,[‡] Xavier Paquez,[†] Cédric Boissière,[†] François Ribot,[†] Clément Sanchez,[†] Corinne Chanéac,[†] and David Portehault*[,†]

[†]Sorbonne Universités, UPMC Univ Paris 06, CNRS, Collège de France, Laboratoire de Chimie de la Matière Condensée de Paris (LCMCP), 11 place Marcelin Berthelot, F-75005 Paris, France and [‡]Sorbonne Universités, CNRS, UPMC Univ Paris 06, Institut des NanoSciences de Paris (INSP), 4 Place Jussieu, F-75005 Paris, France

ABSTRACT Although gold nanoparticles stabilized by organic thiols are the building blocks in a wide range of applications, the role of the ligands on the plasmon resonance of the metal core has been mostly ignored until now. Herein, a methodology based on the combination of spectroscopic ellipsometry and UV–vis spectroscopy is applied to extract dielectric functions of the different components. It is shown that aromatic thiols allow a significant charge transfer at the hybrid interface with the s and d bands of the gold core that yields "giant" red shifts of the plasmon band, up to 40 nm for spherical particles in the size range of 3–5 nm. These results suggest that hybrid nanoplasmonic devices may be designed through the suitable choice of metal core and organic components for optimized charge exchange.

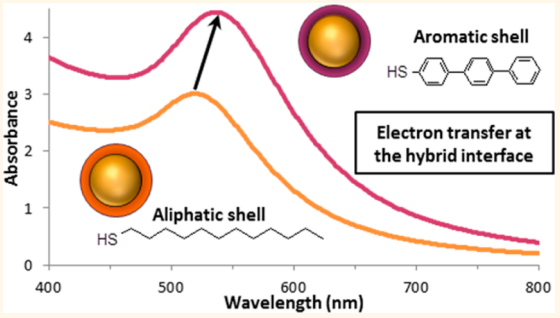

KEYWORDS: gold nanoparticles · aromatic ligands · thiols · plasmonic properties · charge transfer

Gold nanoparticles have reached technological maturity in different fields ranging from nanoelectronics and sensing to biomedicine and catalysis.[1−3] These particles are conveniently produced by colloidal synthesis, meaning reactions between molecule-scale precursors in solvents.[4] Such processes yield nano-objects coated with organic molecules, so-called ligands, which support many desired functions, especially stability *versus* aggregation and dissolution, biocompatibility, and molecular recognition.[5] These ligands are usually thiol molecules covalently bonded to gold atoms[6] and can be described through three components: the headgroup, a sulfur atom coming from the abstraction of a hydrogen radical or a proton from the initial thiol,[7] the side chain that provides steric colloidal stabilization or solubility,[8] and the end group that can be functionalized for, *e.g.*, molecular recognition,[5] click chemistry,[9] or modification of cell adhesion.[10]

The main interest in gold nanoparticles with diameters in the range 3−100 nm lies in their localized surface plasmon resonance that occurs in the visible range and can probe the close environment.[11] On one hand, it can influence the spectroscopic behavior of molecules by Fluorescence Resonance Energy Transfer[12] or by field enhancement as in Surface Enhanced Raman Spectroscopy, thus yielding competitive probes for molecular detection in biological systems, for instance.[13,14] On the other hand, gold nanoplasmonics[15] attracts interest because of the sensitivity of the plasmon resonance to the local environment of the nanostructure. Such a dependency is classically explained by the role of the dielectric constant of the surrounding medium. For instance, it is well-known that an increase in the refractive index of the embedding medium or in the thickness of a shell leads to a red shift in the absorption band.[16] In addition, plasmon coupling between single nano-objects in close proximity can also considerably modify the resonance conditions. In conjunction with the shape sensitivity, this approach is the basis of plasmonic metamaterials.[15,17,18]

Despite these known effects, the role of the ligands themselves on the plasmon resonance of gold nanoparticles has hardly

* E-mail: david.portehault@upmc.fr.

Received for review May 12, 2015 and accepted July 10, 2015.

Published online July 10, 2015
10.1021/acsnano.5b02864

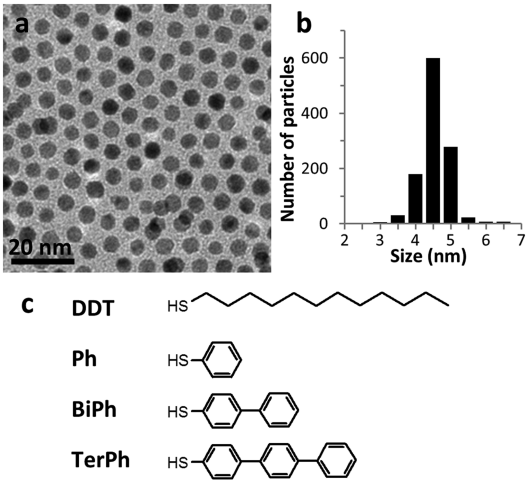

Figure 1. (a) TEM picture of nanoparticles synthesized with DDT. (b) Size distribution of the particles. (c) Chemical structures and abbreviation of the aliphatic and aromatic ligands used in this study.

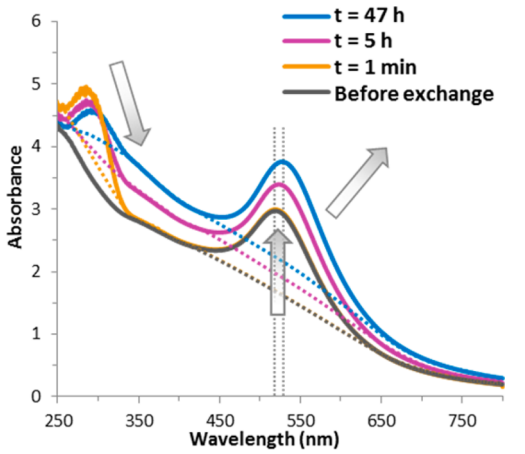

Figure 2. Kinetic evolution of UV−vis spectra of 5 nm nanoparticles, previously stabilized with dodecanethiol during exchange with free TerPh in solution. After 47 h of exchange, the TerPh:DDT composition of the ligand shell is 25:75.

been investigated in the literature. However, such coupling may pave the way to an emerging field where inorganic nanocrystals could be combined with specific organic molecules in order to design hybrid nanoplasmonic devices. The reason for the lack of investigations in this field lies in several factors. First, most organic thiols share similar values of refractive index, so that the classical considerations cited above predict only a small impact on the plasmonic response by changing the grafted molecules. However, it has been recently suggested that specific side chains can modulate the charge transfer between ligands and the gold core,[6,19,20] but the effect of this charge redistribution on the plasmon resonance has not been considered yet. A second reason explaining the absence of studies on plasmonic effects of the side-chain is linked to a methodological limitation. Indeed, if numerical approaches such as the boundary element method, discrete dipole approximation, or plasmon hybridization method allow precise modeling of the optical properties of core−shell metal particles with complex shapes,[21−23] they rely on the knowledge of the frequency-dependent dielectric functions of the different components. Generally speaking, tabulated values for bulk metals are most often used,[21,22] which levels every potential change in the permittivity if charge transfer takes place.

Herein, we present the synthesis and optical properties of hybrid nanoplasmonic systems composed of monodisperse spherical gold nanoparticles covered by aliphatic or aromatic thiolates (Figure 1). We demonstrate the occurrence of charge transfer at the hybrid gold/thiolate interface through its considerable impact on the plasmonic response of the gold core, which exhibits unparalleled wavelength shifts for spherical gold particles. To achieve this goal, we develop a methodology based on the combination of experiments and calculations, which is generalizable to many other metal nanoparticle/ligands couples. Spectroscopic ellipsometry is used to retrieve reliable frequency-dependent dielectric functions of the organic monolayer. The latter are implemented with the parametrization of the gold dielectric function to fit the experimental visible absorption spectra of the nanoparticles that enable assignment of the charge transfer to the different electronic bands of the core. As already suggested by *ab initio* calculations,[6,24] aside from the expected interaction with gold free electron s-band due to the thiolate bond, the analysis demonstrates a spectacular role of the electron transfer on the interband transitions of gold at the hybrid interface.

RESULTS AND DISCUSSION

Nanoparticles of 5 nm in diameter with a narrow size distribution were functionalized by a ligand shell containing two ligands (Figure 1): dodecanethiol (DDT) and an aromatic thiol (ArSH). The bifunctionalized corona was obtained by partial exchange of the initial dodecanethiol with ArSH, namely Ph (phenylthiol), BiPh (p-biphenylthiol), TerPh (p-terphenylthiol).

Optical Properties after Functionalization with Aromatic Thiols: UV−vis Spectrometric Study. Figure 2 shows the time evolution of the UV−vis spectrum of a suspension containing 5 nm gold nanoparticles initially stabilized with DDT when some TerPh is added in solution. Before ligand exchange, the suspension is characterized by a localized surface plasmon band with a maximum at 519 nm, in agreement with the literature.[30] When the aromatic thiol ligand is added, the absorption band related to the $\pi-\pi^*$ electronic transitions in the aromatic cycles appears near 270 nm. Then, as ligand exchange takes place, this absorption band decreases and the absorption background increases (see, *e.g.*, the 350−450 nm region), while the localized surface plasmon band absorption intensity increases and shifts

to higher wavelengths. In this example with a final ligand shell composition TerPh:DDT 25:75 (Figure S1, Supporting Information), a spectacular red shift of the plasmon band occurs up to 527 nm. This value would correspond to nanoparticles of 40 nm by considering only radiative depolarization[31] for a classical ligand shell containing only an alkylthiol.[32] While the plasmon band maximum for pure DDT shell is at 519 nm, in agreement with the literature,[30] both the wavelength and the maximum absorbance are modified by the adsorption of aromatic ligands. In order to ensure that the modification of the optical properties was only due to the grafting of the aromatic thiols, we carefully verified that no modification of size or polydispersity and no aggregation of the particles occurred during ligand exchange (Figure S2). In addition, the homogeneity of the mixed ligands shell was assessed by NOESY NMR experiments in order to probe the close vicinity of the aliphatic and aromatic chains. The results (Figure S3) suggest an intimate mixing between both ligands. Because morphology, size modification of the gold core, aggregation, and nonhomogeneous grafting can be safely ruled out, the evolution of the optical properties is only due to the random grafting of the aromatic ligands.

In order to confirm the observed trends, different particle sizes, shell compositions, and aromatic ligands were studied. Contrary to 5 nm particles which tend to aggregate for TerPh:DDT ratios higher than 25:75, smaller particles show enhanced colloidal stability and can be functionalized by TerPh only, using Brust's method. The corresponding suspensions show similar alterations of their optical properties compared to nanoparticles synthesized with DDT (*i.e.*, a red shift), although the plasmon band is wider in agreement with a smaller diameter (Figure S4).[33] Consequently, changes described above in the optical properties in the presence of aromatic thiol ligands are a phenomenon that can be generalized to different particles sizes, ligand shell compositions, and functionalization processes.

The time evolution of the position of the plasmon band maximum during DDT exchange with different aromatic thiols is reported in Figure 3 for 5 nm particles suspended in chloroform. Again, no aggregation or size modification is observed after exchange (Figure S5). The wavelength at the maximum strongly increases during the first 20 h of the ligand exchange and then stabilizes. The maximum absorbance follows the same trend (Figure S6). These evolutions reflect the kinetics of ligand exchange. For a given pair of ligands, an increase in the content of the aromatic component leads to a stronger red-shift of the plasmon band position and an increase in the related absorbance. The number of aromatic rings in the ArSH ligand also impacts the optical properties. For instance, when the shell composition is changed from Ph:DDT (41:59) to BiPh:DDT (50:50) and TerPh:DDT (50:50), the plasmon

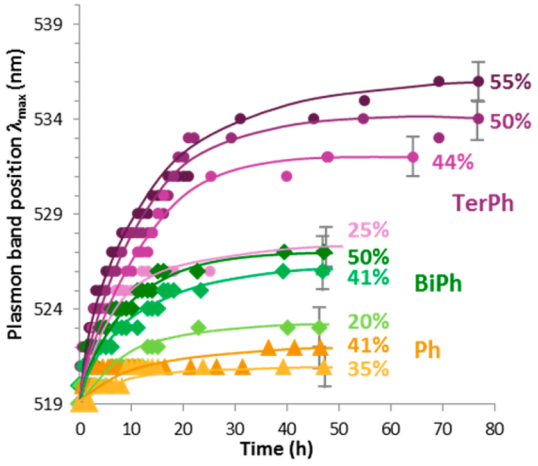

Figure 3. Time evolution of the plasmon band position during ligand exchange of DDT with Ph, BiPh. and TerPh. The percentages are the measured final proportions of aromatic ligands on the gold nanoparticles surface.

band shifts from 522 to 527 and 534 nm, respectively, while the absorbance is 10%, 23%, and 47% stronger than with DDT only. Thus, for a similar DDT:ArSH composition, the more adjacent cycles in the aromatic thiol, the stronger the absorbance and the more red-shifted the maximum of the plasmon band.

The role of the near environment of metal particles on the plasmonic response is well-known in the literature.[21,16] Maxwell's equations provide the general framework for the comprehension of this dependency, especially their analytical solutions derived for spherical particles smaller than the incident wavelength.[34] In the far-field regime, at visible wavelengths and for nanoparticles smaller than ~10 nm, the extinction cross section is mainly driven by absorption while scattering is negligible.[31] The dipolar contribution to the absorption cross section C_{abs} per particle depends on the particle polarizability α:[31]

$$C_{abs} = \frac{2\pi}{\sqrt{\varepsilon_m}} \frac{\mathrm{Im}(\alpha)}{\lambda} \quad (1)$$

For a gold−ligand core−shell particle (Figure 4a), where the core has a permittivity ε_g and radius R_g, the ligand shell has a permittivity ε_l and a thickness $R_l - R_g$, and the embedding medium has a permittivity ε_m[21,35]

$$\alpha = \alpha_{core-shell} = 4\pi R_1^3 \varepsilon_m \frac{(\varepsilon_l - \varepsilon_m)(\varepsilon_g + 2\varepsilon_l) + f(\varepsilon_m + 2\varepsilon_l)(\varepsilon_g - \varepsilon_l)}{(\varepsilon_l + 2\varepsilon_m)(\varepsilon_g + 2\varepsilon_l) + 2f(\varepsilon_l - \varepsilon_m)(\varepsilon_g - \varepsilon_l)} \quad (2)$$

with

$$f = \left(\frac{R_g}{R_l}\right)^3$$

Equation 2 has already been successfully used to predict the position of the absorption maximum of gold−silica core−shell particles.[36] The dielectric modeling is well adapted since the size range explored

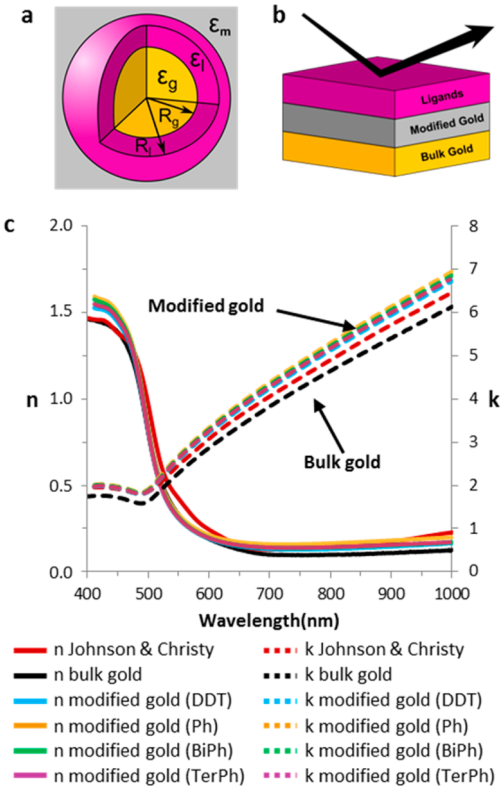

Figure 4. (a) Schematic representation of a gold nanoparticle (dielectric function ε_g) with a ligand shell (ε_l) embedded in a surrounding medium (ε_m). The radii R_g, R_l and dielectric functions of the different media ε_g, ε_l, and ε_m are used in the analytic expression of the absorption cross-section to simulate the absorbance spectra of the nanoparticles. (b) Scheme of the three-layer model used to fit the ellipsometric data. (c) Optical functions *n* and *k* obtained from the fit for bulk gold (with no ligand layer) and for the modified gold buffer layer. The analysis was performed for each ligand.

herein is far beyond that of the birth of localized surface plasmon, without any molecular level splitting in the gold core as observed in small clusters.[24] Frequency-dependent dielectric functions of bulk gold and of the chloroform solvent (ε_m) are available in the literature,[37,38] but not those of the ligands (ε_l). In addition, the permittivity of gold (ε_g) in small particles may be impacted by finite-size effects[39] and by the charge transfer with the ligands owing to the high surface/volume ratio. In order to obtain reliable parameters for absorbance spectra analysis, spectroscopic ellipsometry was used to retrieve the dielectric functions and thicknesses of the ligand shells (ε_l, $R_l - R_g$).

Optical Properties of the Aromatic Ligand Shells: Spectroscopic Ellipsometry. Self-assembled monolayers (SAMs) of DDT, Ph, BiPh, and TerPh were prepared on atomically flat gold (111) substrates. According to X-ray photoelectron spectroscopy (XPS), the grafting densities were estimated around 5 ligands/nm^2, in agreement with reported data for gold planar surfaces and nanoparticles.[40,41] These films were used as models for the determination of the optical properties of the

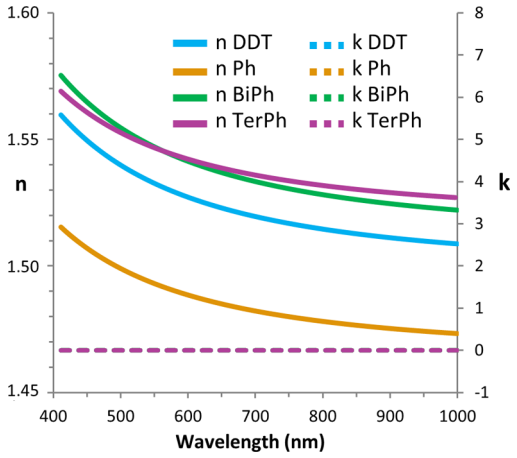

Figure 5. Optical functions *n* and *k* obtained for the ligands monolayers on the gold substrate with the three-layer model. All *k* values of the ligands are 0, so that the dashed lines are superimposed.

organic layer by recording ellipsometry spectra at various incident angles. Attempts to fit the data with a two-layer model, made of the bulk gold substrate analyzed before thiol coating, and a layer of thiol, were unsuccessful and yielded inconsistent results, which suggested that the organic layer was more electrically conductive than the bulk gold substrate (Figures S7−8 and Table S1). These unrealistic results oriented the analysis toward a three-layer model. This model (Figure 4b) comprises a first bulk gold layer that has the same optical properties as those obtained for the gold substrate with no grafted ligands and in agreement with already reported data.[38] The outer layer made of the organic SAM has a dielectric behavior, which obeys a classical Cauchy behavior. The added intermediate buffer layer consists in gold with a dielectric behavior different from the bulk (Figure 4c). A fit of the ellipsometry data gives a 16 nm thick buffer layer of modified gold with higher *n* and *k* values than the bulk (Figure 4c). The Drude component of this buffer layer shows an increase by 20% of the density of charge carriers and a decrease by 33% of their mobility (Figure S9). Thus, grafting a thiol on a gold surface, whatever its aromatic or aliphatic nature, leads to the formation of a modified gold layer which is more absorbent and enriched in conduction electrons than bulk gold. This same three-layer model yields the optical properties of the SAM for each thiol (Figure 5). The thicknesses for the DDT, Ph, BiPh, and TerPh SAMs are1.2, 0.6, 0.8, and 1.2 nm, respectively, in agreement with the literature.[42] The optical indexes *n*, near 1.5, agree with tabulated data[43] and are reasonable for organic compounds. The extinction coefficients *k* are zero showing that the ligands do not absorb light in the studied wavelength domain. This purely dielectric behavior matches with the presence of the $\pi-\pi^*$ transitions in the aromatic ligands only at wavelengths shorter than 350 nm (Figure 2).

TABLE 1. Experimentally Determined Wavelength of the Plasmon Band Maximum (λ_{max}) for 5 nm Diameter Nanoparticles Functionalized with Different Ligand Shells and Calculated Values of λ_{max} from Different Dielectric Functions of Gold

ligands (shell composition)	exptl value (nm)[a]	calcd from tabulated gold (nm)[b]	calcd from bare gold (nm)[c]	calcd from modified gold (nm)[d]
DDT (100%)	519	533	541	524
Ph:DDT (35:65)	521	530	538	519
BiPh:DDT (50:50)	528	532	541	523
TerPh:DDT (50:50)	535	533	542	524

[a] From UV−vis spectra of the suspensions. [b] ε_g^{tab} obtained from ref 38. [c] ε_g^{bulk} obtained from spectroscopic ellipsometry. [d] ε_g^{DDT}, ε_g^{Ph}, ε_g^{BiPh}, and ε_g^{TerPh} obtained from spectroscopic ellipsometry.

Spectroscopic ellipsometry provides the dielectric functions (ε_l) and the thicknesses ($R_l - R_g$) of the organic layers to be implemented in the calculation of the absorption cross section C_{abs} for core−shell nanoparticles. In addition, it also suggests that grafting thiol ligands strongly affects the optical properties (ε_g) of gold near the surface. Since for the planar SAMs geometry this modification propagates over a thickness of 16 nm, even more drastic modifications are to be expected in the finite volume of particles of 5 nm in size. Nevertheless, the data obtained by ellipsometry show qualitatively that the transport properties of gold in the vicinity of the ligands are modified compared to bulk gold.

Simulation of the Absorption Spectra of Gold Nanoparticles with Dielectric Functions Experimentally Determined by Ellipsometry. The absorption spectra of the 5 nm nanoparticles covered with each kind of ligands were first simulated using the analytical expression of C_{abs} eqs 1 and 2 with the dielectric functions and thicknesses of the ligands layers (ε_l, $R_l - R_g$) extracted from ellipsometry measurements. Different gold permittivities (ε_g) were compared, including optical properties of bulk gold (from tabulated data ε_g^{tab} [38] or ellipsometric measurements on the bare substrate ε_g^{bulk}) and of the modified buffer 2D layers for DDT, Ph, BiPh, and TerPh (ε_g^{DDT}, ε_g^{Ph}, ε_g^{BiPh}, and ε_g^{TerPh}, respectively). Calculated and experimental values of the plasmon band maximum wavelength are reported in Table 1. Values originating from the modified gold layers or tabulated values are closer to experimental ones, but the increase with the number of aromatic cycles observed experimentally (see Figure 3) cannot be reproduced from these simple calculations. Indeed, finite-size effects in the nanoparticles likely lead to a modification of the dielectric function ε_g compared to the 16 nm-thick planar layer. The grafting densities on flat gold substrates and on gold nanoparticles were measured by XPS and NMR through the iodine death reaction,[28] respectively, and were both around 5 ligands/nm^2. By considering this value, the 16 nm-thick gold layer below flat SAMs comprises one thiol molecule for 190 gold atoms, whereas nanoparticles of 5 nm exhibit one thiol for only 10 gold atoms. Considering the optical functions of the ligand monolayers and their eventual dependence on the planar/nanoparticles geometries, they should be more impacted by charge transfer in the planar configuration, with a deeper gold sink. Nevertheless, ellipsometric data show that this geometry (Figure 5) yields n and k values close to the expected ones for pure bulk ligands, thus suggesting a poor influence of the geometry on the optical properties of the organic layer and validating the use of ellipsometry-derived functions for the nanoparticles. In addition, if charge transfer were changing significantly optical properties of the organic layer, it should impact mainly its absorption, in other words, the imaginary part of the dielectric function, which shows sizable values ($k \neq 0$) only in the $\pi-\pi^*$ transition region, outside the wavelength range probed by spectroscopic ellipsometry and far from the plasmon resonance. The electronic modification due to the ligand shell is therefore spread over a smaller amount of gold matter, which causes more important changes in the metal dielectric function. The deviation between the planar semi-infinite geometry and the confined spherical one may arise from different physical effects, including the increasing damping rate of the conduction electrons due to surface scattering or electron transfer between gold and the ligands. The former is usually mentioned to explain the size-dependency of the absorption maximum in suspensions of gold nanoparticles of varying diameter.[39] However, it fails to describe the strong shifts observed for different ligands with the same particle size and with the same grafting head. This trend suggests an influence of each ligand on the dielectric function of nanoscaled gold. To evaluate this impact, the experimental absorption spectra of the suspensions were modeled with the purpose of determining the actual dielectric function of confined gold for each ligand.

Analysis of the Absorption Spectra of Gold Nanoparticles: The Dielectric Function of Gold Confined in a Ligand Shell. The absorption spectra were fitted with eqs 1 and 2. Ellipsometry measurements described above were used only to provide the dielectric functions and thicknesses of the ligand shells (ε_l, $R_l - R_g$) (Figure 6), assuming that the dielectric function of the ligand shell of the particles is equivalent to the dielectric function of the planar self-assembled monolayer.

To handle the effect of ligands and confinement on the gold dielectric function, this latter ε_g was parametrized accordingly to[44]

$$\varepsilon_g(\omega) = \varepsilon_\infty - \frac{\omega_D^2}{\omega^2 - i\omega\Gamma_D} + G_1(\omega) + G_2(\omega) \quad (3)$$

where $\omega = 2\pi c/\lambda$ is the optical angular frequency (c the speed of light). The two first terms describe the Drude intraband transitions related to the conduction electrons (s electrons). ε_∞ is the dielectric function at high frequency and ω_D the Drude plasma frequency

$$\omega_D = \sqrt{\frac{n_s e^2}{m_e \varepsilon_0}} \quad (4)$$

which is related to n_s, the density of free carriers, m_e, the electron mass, and e, the elementary charge. Γ_D is a phenomenological damping of the conduction electrons. In the field of gold colloid plasmonics, the Drude or free-electrons contribution is usually the only one considered to account for the shape and position of the plasmon band.[21] In particular, the broadening of the plasmon band when the particle diameter decreases in the range 2−10 nm is described only by a size-dependent damping rate Γ_D, due to an enhanced surface scattering, which scales with the surface/volume ratio.[36] However, and contrary to silver,[45] the screening of conduction electrons by the more localized d electrons in gold cannot be neglected in the visible/near-UV region since the two interband 5d → 6sp transitions at 330 and 470 nm overlap with the localized surface plasmon. This results in a sizable discrepancy between the Drude model and the absorption profile when interband transitions are neglected (Figure S9b). For this reason, the two main interband transitions $G_1(\omega)$ and $G_2(\omega)$ centered at 470 and 330 nm, respectively, have been accounted for by using the critical point transition approach for dipolar transition[44]

$$G_i(\omega) = \frac{C_i e^{i\Phi_i}}{(\omega_i - \omega - i\Gamma_i)^{\mu_i}} + \frac{C_i e^{-i\Phi_i}}{(\omega_i + \omega + i\Gamma_i)^{\mu_i}} \quad (5)$$

where $\omega_i/2\pi$ are the frequencies of the interband transitions. Γ_i are the corresponding dampings, while C_i, Φ_i, and μ_i are, respectively, the amplitudes, the phases, and the pole orders of the transitions, while Φ_1 and μ_1 are fixed at $-\pi/4$ and = 1, respectively.[44] $G_i(\omega)$ is a convenient generalization of oscillator-like transitions that includes the effects of reciprocal space integration on the line shape and the broadening of a given solid state transition.[46] The complex dielectric function of the bare gold substrate obtained by spectroscopic ellipsometry is satisfactorily modeled by eq 3 (Figure S10 and Table S2, Supporting Information) and yields ε_∞, ω_D, τ_D, ω_i, Γ_D, C_i, and μ_i parameters (Table 2) in reasonable agreement with the published fits of the data from Johnson and Christy.[38,44]

Before fitting actual absorbance spectra, it is useful to schematically describe the impact of the different parameters of $G_1(\omega)$, the transition closest in wavelength to the plasmon resonance. Calculations performed for a spherical particle into chloroform without any shell (Figure S11) show that increasing ω_D leads to a blue shift of the plasmon resonance, while Γ_D does not impact the position of the plasmon band but only its broadening.[21] From the interband transitions viewpoint, decreasing ω_1 results in a blue shift and narrowing of the plasmon band. Increasing Γ_1 leads to a blue shift and broadening, while increasing the interband strength C_1 yields mostly a red shift, with only minor impact on the broadening. Accordingly, without

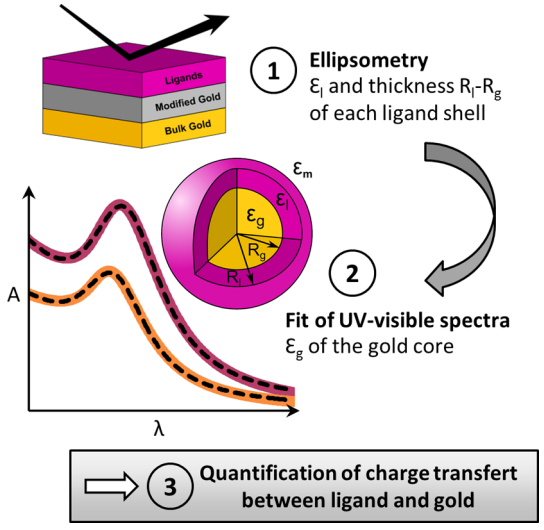

Figure 6. Methodology developed to understand plasmon resonance shifts in hybrid core−shell nanoparticles and to highlight and quantify charge transfer between the ligand shell and the core of nanoparticles.

TABLE 2. Parameters Deduced from the Fits of the Absorption Spectra of Gold Nanoparticle Suspensions

shell (composition)	$\hbar\omega_D \pm 0.02$ (eV)	$\hbar\Gamma_D \pm 0.004$ (eV)	$\hbar C_1 \pm 0.06$ (eV)	$\hbar\omega_1 \pm 0.02$ (eV)	$\hbar\Gamma_1 \pm 0.005$ (eV)	$\hbar\omega_B \pm 0.02$ (eV)
bare gold substrate[a,b]	8.22	0.082	2.29	2.67	0.540	3.49
DDT (100%)	8.85	0.577	2.42	2.68	0.601	3.60
Ph:DDT (50:50)	8.83	0.569	2.50	2.68	0.609	3.66
BiPh:DDT (50:50)	8.84	0.591	2.86	2.68	0.634	3.92
TerPh:DDT (50:50)	8.77	0.625	2.97	2.67	0.624	3.99

[a] Direct fit of the dielectric function obtained from spectroscopic ellipsometry. [b] Parameters for the second interband transition $G_2(\omega)$ have been adjusted during the direct fit of this dielectric function, yielding ω_2, Γ_2, and C_2 that were then used as constants for the fit of the absorption spectra of the nanoparticles: $\hbar\omega_2 = 3.779$ eV, $\hbar\Gamma_2 = 1.261$ eV, $\hbar C_2 = 4.963$ eV. $\omega_B = (2\omega_1 C_1)^{1/2}$.

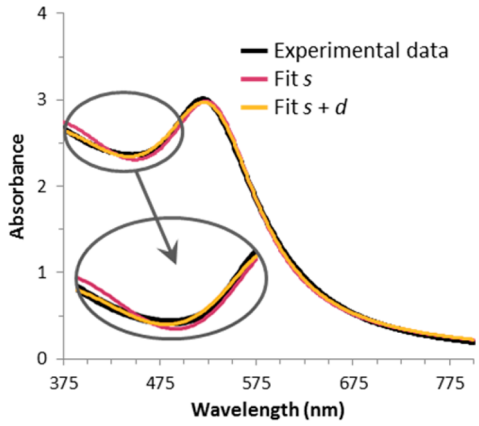

Figure 7. Experimental UV−vis spectrum of a DDT-stabilized gold suspension with fit curves taking into account only intraband transitions (*s*) or the intraband and the interband transitions G_1 (*s* + *d*).

adjustment, one can already foresee that the damping rate of conduction electrons Γ_D cannot explain alone the observed red shift with constant bandwidth for an increasing number of aromatic cycles in the ligand chain.

To model the behavior of the core−shell nanoparticles, ε_∞, ω_2, Γ_2, and C_2 ($G_2(\omega)$ parameters) have been fixed at their bulk values since they correspond to deep lying transitions which cannot interact with the plasmon resonance. Regarding the dielectric function ε_1 of mixed shells, a simple mixture law was used accordingly to the experimentally determined surface composition. Only ω_D, Γ_D, ω_1, Γ_1, C_1, and a scale factor have been used to reproduce the experimental spectra. The adjustment for the particles covered only by DDT is shown in Figure 7 and compared with a fit where the interband transition $G_1(\omega)$ has been fixed at its bulk value, and only ω_D, Γ_D, and the scale factor are adjusted. For all ligands (Figure S12 and Table S3, Supporting Information), the only way to reproduce satisfactorily the experimental line shape and position is to adjust, together with the intraband transitions, the dielectric contribution from the interband $G_1(\omega)$ transition, suggesting that it plays an important role in the nanoparticles optical properties. Parameters obtained from the fit are gathered in Table 2.

The above analysis which assigns a strong weight of both s and d electrons on the observed plasmon shift from one ligand to the other relies on the transferability of the dielectric function of the SAMs measured by ellipsometry to ligand shells. However, attempts to fit experimental nanoparticle absorbance spectra with only s-electron contributions (*i.e.*, ω_D, Γ_D) and with an adjustable shell dielectric function led to discrepancies similar to those of Figure 7 but, more importantly, to absorbing shell refractive indexes not compatible with an organic layer as in the case of the fit of the SAMs ellipsometry data with the two-layer model. To reinforce the analysis, spectra (Figure S13) have been simulated over the whole spectral range (200−800 nm) with the fitted parameters of Table 2 (range 375−800 nm). The agreement below 375 nm for DDT validates the absence of $G_2(\omega)$ modification due to grafting. Analogously, a similar agreement for aromatic ligands (Figure S13b−d) could be obtained down to $\pi-\pi^*$ transitions by summing the simulation with the absorbance of the ligands alone in solution corrected from a dilution ratio.

Finite-Size Effects on the Plasmon Resonance. The increase in ω_D by going from the gold layer to the confined thiol-bounded nanoparticles indicates an increase in the amount of s electrons contributing to the plasmon band. Thus, grafting thiols on a gold nanoparticle enriches in an effective way the core in free electrons. The increase in the damping rate Γ_D from a layer to a nanoparticle is a consequence of the confinement of the free electrons in the nanoparticle. The latter can be described by a size-dependent damping rate[31,36]

$$\Gamma_D = \Gamma_D^{bulk} + Av_F/R \qquad (6)$$

where v_F is the Fermi velocity, R is the particle radius, and A is a geometric factor close to unity. In our case, eq 6 gives $\hbar\Gamma_D \approx 0.45$ eV ($A = 1$), in agreement with the fit, although the larger experimental values may be due to an additional interfacial chemical damping.[47] On the contrary, interband transition energy ω_1 and damping Γ_1 are poorly affected by the finite-size, in agreement with the more localized character of the *d* electrons.

Role of the Binding Group on the Plasmon Resonance of Gold Nanoparticles. Equation 4 relates the variation of the density of conduction s electrons of each core−shell particles to the observed change in plasma frequency, *i.e.*, $\Delta n/n = \Delta\omega_D/2\omega_D$. By considering that each gold atom ($5d^{10}\ 6s^1$) provides one s electron and that one particle of 5 nm diameter contains *ca.* 4000 Au atoms, the core itself provides *ca.* 4000 s electrons. The additional s electrons deduced from ω_D are attributed to the enrichment of the core from the ligands. According to the grafting density of 5 thiol/nm^2,[40,41] and by correcting the relative amount of aromatic ligands in the mixed shells, the number of s electrons transferred from each type of ligand can be evaluated (Figure 8). Each thiol provides on average 1.2 s electrons to the core. This enrichment matches the ellipsometry data on planar surfaces. The direction of charge transfer is in agreement with our experimental conditions where ligand binding occurs first by deprotonation of the thiol group.[29] The observed transfer of *ca.* 1 s electron agrees with the formation of a covalent bond between a gold atom and the resulting thiolate.[29] The negative charge is transferred to the core, and this additional electron contributes to the collective plasmon oscillation.

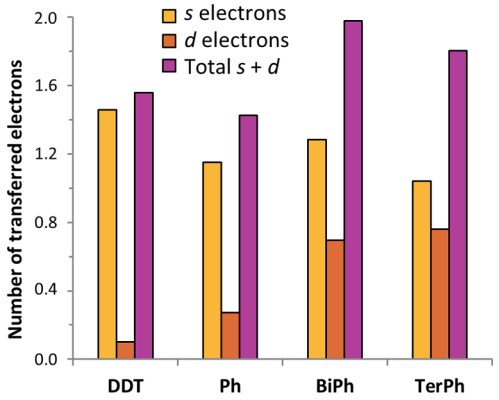

Figure 8. Quantity of electrons transferred per molecule for each ligand to the gold core.

Effect of the Thiol Side-Chain Nature. When considering the nanoparticles, the amplitude of the interband transition C_1 is the most impacted parameter by a change in the ligand shell (23% changes among the different shell compositions). Since the transition pole order μ_1 is one, the G_1-parameters can be combined to yield the plasma frequency ω_B of the transition, in other words, its oscillatory strength $\omega_B = (2\omega_1 C_1)^{1/2}$. The increase in the amplitude C_1 results in a significant modification (11%) of the oscillatory strength ω_B when going from a pure DDT shell to the mixture TerPh:DDT 50:50. In analogy with eq 4,[43] the number of involved d electrons n_d in the transition is then given by

$$\frac{n_d}{n_s} = \frac{\omega_B^2}{\omega_D^2} \quad (7)$$

Following the same reasoning made previously for s electrons, eqs 4 and 7 yield the number of d electrons mobilized per thiol molecule (Figure 8). For DDT, the electrons transferred at the hybrid gold/thiol interface mostly have an s nature. For aromatic ligands, the amount of d electrons involved in the hybridization between ligand molecular orbitals and the gold core increases as the ligand contains more adjacent aromatic cycles. In parallel, the s electron contribution is slightly reduced. Thus, when charge delocalization is facilitated by increasing the number of adjacent aromatic cycles, the nature of the electronic transitions in the gold core is modified: intraband transitions (s electrons) are less important, whereas the interband transitions (d electrons) are intensified with a corresponding increase in the density of d electrons in the gold core, leading to a shift of the localized plasmon band resonance and a strong increase of the absorbance (Figure 2). Therefore, the side chain of the ligands has an undisputable effect on the optical properties of the core. This phenomenon does not arise from changes in the dielectric constant of the ligand shell itself but from modifications of the dielectric properties of the core, thus highlighting charge transfer at the hybrid interface between the ligand chains and the core. Importantly, classical approaches focusing only on the dielectric properties of the surrounding medium would be unsuccessful to stress such effects because the permittivities of the organic thiols are very similar.

CONCLUSION

This study evidenced that current methods used to model the plasmonic response of gold nanostructures can be flawed, especially when charge transfer takes place at interfaces of gold nano-objects with an organic medium. Indeed, all previous works rely on the tabulated dielectric properties of pure ligands and gold in the bulk state with some modulation of the electron relaxation time. This represents a strong limitation as soon as one of the components (*e.g.*, ligands) influences the optical properties of the others (*e.g.*, gold core). To overcome this bottleneck, we developed an original approach (Figure 6) that relies on the experimental determination of the optical constants of the shells, by spectroscopic ellipsometry, assuming that they are similar to those of the corresponding planar SAMs. These constants are used to fit experimental absorption spectra of the nanoparticles, which yield the actual dielectric function of the metal core through a suitable parametrization. This methodology allows highlighting the complex picture of charge transfers at thiol/gold interfaces and how they impact the electron populations in the metal nano-objects. It should be applicable to a wide range of ligand-protected nanoparticles based on a gold or silver core, with shells consisting of various organic ligands or dielectric media, and also other metals or alloys.

This method was successfully applied herein to gold nanoparticles stabilized by thiol ligands and obtained by colloidal synthesis. A spectacular modification of the plasmonic properties of the gold cores by aromatic thiols was evidenced, with the arising of an unprecedented "giant" red shift, up to 40 nm, of the plasmon resonance. Changes in the plasmonic response of gold nanoparticles stem from charge transfer from the side chain of the grafted thiolates to the metal core, which results in a redistribution of electron populations in the gold nanoparticles. Therefore, from an electronic perspective, the classical view of gold nanocrystals as finite pieces of bulk metal is too restrictive, as already highlighted for smaller gold clusters showing a semiconductor behavior.[48] On the contrary, thiol-grafted gold nanoparticles should be envisioned as genuine organic–inorganic nanostructures where the hybrid interface can be the locus of extensive charge transfer. This approach enables to envision an alternative development of hybrid nanoplasmonics, where the electronic properties of gold nanodomains will be finely tuned by the controlled injection of electrons from a smartly chosen ligand shell, thus allowing a

drastic economy of gold atoms: 5 nm colloids smartly functionalized have a similar absorption spectrum than 40 nm particles but involve 500 times less atoms. In addition, some smart sensors based on the perturbation of the electronic properties of the ligand shell, then on the ligand/gold electronic coupling, are likely to be very sensitive to many external chemical and physical solicitations.

EXPERIMENTAL SECTION

All chemicals were purchased from Sigma-Aldrich and used as received.

Nanoparticle Synthesis. Gold nanoparticles were synthesized using a method described by Stucky *et al.*[25] and modified by Pileni *et al.*[26] Briefly, $AuCl(PPh)_3$ (300 mg, 1 equiv) was dissolved in 60 mL of toluene with dodecanethiol (1.16 mL, 8 equiv). The solution was stirred at 100 °C for 5 min, and a preheated solution of *tert*-butylamine borane complex (526 mg, 10 equiv) in 36 mL of toluene was added. The mixture was stirred at 100 °C for 3 min and then cooled at room temperature. The gold nanoparticles were precipitated with ethanol and centrifuged. Four cycles of redispersion in toluene (1 mL), precipitation with ethanol (20 mL), and centrifugation were performed. The particles were finally redispersed in 80 mL of toluene. The suspension was divided into 5 mL batches and dried. The diameter of the particles was evaluated to 4.8 nm ±0.4 nm according to transmission electron microscopy (TEM) measurements on 1130 particles (Figure 1).

Smaller nanoparticles of 3.5 nm were also investigated and functionalized only by TerPh. These particles were also synthesized by the classical Brust−Schiffrin protocol.[27] Briefly, $HAuCl_4{,}3H_2O$ (30 mg, 1.0 equiv) was dissolved in 2.25 mL of water and extracted with a solution of tetraoctylammonium bromide (92.5 mg, 2.2 equiv) in 1.71 mL of toluene. The aqueous layer was removed and a solution of TerPh (*p*-terphenylthiol, 5.5 mg, 0.3 equiv) in 0.53 mL of toluene was added. The mixture was stirred and cooled at 0 °C, and 2.1 mL of a cold $NaBH_4$ solution (0.36 M, 10.0 equiv) was added quickly under vigorous stirring. After 3 h at room temperature, the aqueous layer was removed, the organic layer was washed with water, and the particles were precipitated with ethanol and centrifuged. They were washed by four consecutive cycles of redispersion in toluene (1 mL), precipitation with ethanol (20 mL), and centrifugation and were finally dispersed in chloroform.

Transmission Electron Microscopy (TEM). TEM observations were performed on a Tecnai Spirit G2 microscope operating at 120 kV. The nanoparticles were deposited onto carbon-coated copper grids from diluted chloroform suspensions and then dried in air.

UV−vis Kinetics. The absorbance spectra were recorded with an Agilent Technologies Cary 5000 spectrometer. A batch of dried nanoparticles was dispersed into 50 mL of chloroform. The suspension was transferred in a closed quartz cuvette, and its absorption spectrum was recorded between 250 and 800 nm with 1 nm step. Then a small amount of aromatic thiol (typically around 1 mg) was added, the mixture was stirred for 1 min and put in the spectrometer, and a series of spectra was recorded with the closed cuvette until the maximum absorbance reached a steady value.

Determination of the Surface Composition. The detailed procedure is schematically described in the Supporting Information (Figure S1). The maximum absorbance of one batch, containing only dodecanethiol as ligand, was recorded after redispersion in 50 mL of $CHCl_3$. The suspension was then dried under vacuum, and the recovered solid was redispersed in 1 mL of $CDCl_3$ to be quantitatively transferred into an NMR tube. A small quantity of iodine (ca. 5 mg) was added to desorb the ligands from the surface and oxidize them into disulfide species.[28] The ^{1}H NMR spectrum was then recorded, and the quantity of grafted dodecanethiol initially contained in the batch was determined by comparison with the ^{1}H spectrum of a dodecanethiol solution of known concentration. Thanks to this preliminary calibration, it was possible to measure the initial quantity of dodecanethiol in each batch of identical nanoparticles by simply measuring the UV−vis absorbance of its plasmon band. The other batches were redispersed in 50 mL of $CHCl_3$ and were exposed to ligand exchange followed by UV−vis spectroscopy. Then, the suspensions were concentrated to a 1 mL volume of $CHCl_3$, and the particles were precipitated with ethanol. At least three cycles of redispersion (with 1 mL of toluene) and precipitation (with 20 mL of ethanol) were performed to get rid of the free ligands. The suspensions were then dried under vacuum, and the particles were redispersed in $CDCl_3$ to be quantitatively transferred into an NMR tube. Again, iodine was used to free the ligands and measure the remaining quantity of dodecanethiol left on the surface at the end of the exchange. For each sample, the plasmon band absorbance before ligand exchange was used to calculate the exact initial quantity of dodecanethiol contained in the batch. The 1:1 stoichiometry of ligand exchange, commonly described in the literature for a range of thiols,[29] was verified in our case by monitoring by liquid ^{1}H NMR the total amount of free species (DDT and aromatic thiol) in the reaction medium immediately after addition of the aromatic ligand and once the steady state of exchange was reached (stable UV−vis spectrum). The total amount of free species remains constant, thus confirming the 1:1 stoichiometry. The difference between the initial and the final quantities of DTT on the surface was attributed to the aromatic thiol, and the final composition of the surface was so deduced, according to a 1:1 exchange.

Self-Assembled Monolayer Preparation. Flame-annealed 200 nm thick gold deposits on glass were used as substrates for ellipsometry measurements. They were cleaned with water and ethanol, dried under nitrogen, and immersed in a 4 mM solution of thiol for 2 h. Further washing with ethanol was followed by immersion in chloroform for 20 h. The grafted substrates were then thoroughly washed with chloroform and dried under nitrogen. Ellipsometry measurements were performed immediately after drying.

X-ray Photoelectron Spectroscopy. Spectra were recorded on a Omicron Nanotechnology spectrometer equipped with an hemispherical detector and an Al Kα source monochromated at 1486.7 eV. The surface coverage of the thiol molecules on the gold substrate was evaluated from the relative intensities of the Au 4f and S 2p signals, balanced by the respective transmission coefficients (14.061 and 14.18 for Au 4f and S 2p, respectively) and the photoionization cross sections (17.10 and 1.68 for Au 4f and S 2p, respectively). Slight amounts of oxidized sulfur were not considered.

Ellipsometry. Thiol SAMs were analyzed with a M-2000U Woollam ellipsometer at several angles (65°, 70°, and 75°) in the range of 400−1000 nm. The fit of the amplitude ratio and phase shift, as functions of the wavelength, provides access to layer thicknesses and to the real $n(\lambda)$ and imaginary $k(\lambda)$ components of the index of refraction as functions of the wavelength λ. The complex dielectric functions $\varepsilon(\lambda)$ was deduced from $\varepsilon(\lambda) = [n(\lambda) + ik(\lambda)]^2$. First, the exact optical properties of the bare gold substrate were determined using a substrate model considered as a semi-infinite layer in the direct wavelength-by-wavelength inversion of the Mueller matrix. After deposition of SAMs, a two-layer (gold/dielectric) model failed to describe the resulting stack. As a consequence, a three-layer model made of bulk gold/modified gold/dielectric layers was implemented using a simple Cauchy index for the adsorbed organic ligands. The fit of the amplitude ratio and phase shift, as functions of the wavelength, provides access to the complex refractive indexes and to the thicknesses of the buffer and organic layers. The optical properties of the modified gold layer was described using a Gen-Osc package containing a Drude and

three Gaussian models for describing intraband and interband transitions, respectively.

Fits and Calculations of the Absorbance Spectra. Experimental UV−vis absorbance spectra of the grafted particles were fitted in the range 375−800 nm using core−shell dielectric model in the quasi-static approximation. The refractive indexes of the ligand shell obtained by ellipsometry were used as an input while the gold dielectric function was parametrized with Drude and interband transitions following a critical point transition approach.

Conflict of Interest: The authors declare no competing financial interest.

Supporting Information Available: Size distributions of the nanoparticles before and after ligand exchange, evolution of the maximum absorbance at the maximum in the UV−vis spectra during ligand exchange, modifications of the substrate transport properties upon ligand grafting, dielectric function for a bare gold substrate measured by spectroscopic ellipsometry, simulations of interband transition parameters on absorbance spectra, fits of experimental absorbance spectra, and corresponding reliance factors. The Supporting Information is available free of charge on the ACS Publications website at DOI: 10.1021/acsnano.5b02864.

Acknowledgment. The authors acknowledge Vincent Humblot and Claire Valotteau from Laboratoire de Réactivité de Surface (Sorbonne Universités, UPMC Univ Paris 06) for the preparation of the gold substrates for ellipsometry, and Christophe Calers from Institut des Matériaux de Paris Centre for XPS measurements. This work was funded by the C'Nano Ile de France DIM Nano-K under the project NaJaH.

REFERENCES AND NOTES

1. Murray, R. W. Nanoelectrochemistry: Metal Nanoparticles, Nanoelectrodes, and Nanopores. *Chem. Rev.* **2008**, *108*, 2688–2720.
2. Dreaden, E. C.; Alkilany, A. M.; Huang, X.; Murphy, C. J.; El-Sayed, M. a. The Golden Age: Gold Nanoparticles for Biomedicine. *Chem. Soc. Rev.* **2012**, *41*, 2740–2779.
3. Dykman, L.; Khlebtsov, N. Gold Nanoparticles in Biomedical Applications: Recent Advances and Perspectives. *Chem. Soc. Rev.* **2012**, *41*, 2256–2282.
4. Daniel, M.-C.; Astruc, D. Gold Nanoparticles: Assembly, Supramolecular Chemistry, Quantum-Size-Related Properties, and Applications toward Biology, Catalysis, and Nanotechnology. *Chem. Rev.* **2004**, *104*, 293–346.
5. Lévy, R.; Thanh, N. T. K.; Doty, R. C.; Hussain, I.; Nichols, R. J.; Schiffrin, D. J.; Brust, M.; Fernig, D. G. Rational and Combinatorial Design of Peptide Capping Ligands for Gold Nanoparticles. *J. Am. Chem. Soc.* **2004**, *126*, 10076–10084.
6. Häkkinen, H. The Gold−sulfur Interface at the Nanoscale. *Nat. Chem.* **2012**, *4*, 443–455.
7. Caragheorgheopol, A; Chechik, V. Mechanistic Aspects of Ligand Exchange in Au Nanoparticles. *Phys. Chem. Chem. Phys.* **2008**, *10*, 5029–5041.
8. Mei, B. C.; Susumu, K.; Medintz, I. L.; Delehanty, J. B.; Mountziaris, T. J.; Mattoussi, H. Modular Poly(ethylene Glycol) Ligands for Biocompatible Semiconductor and Gold Nanocrystals with Extended pH and Ionic Stability. *J. Mater. Chem.* **2008**, *18*, 4949.
9. Boisselier, E.; Salmon, L.; Ruiz, J.; Astruc, D. How to Very Efficiently Functionalize Gold Nanoparticles by "Click" Chemistry. *Chem. Commun.* **2008**, 5788–5790.
10. Kuna, J. J.; Voïtchovsky, K.; Singh, C.; Jiang, H.; Mwenifumbo, S.; Ghorai, P. K.; Stevens, M. M.; Glotzer, S. C.; Stellacci, F. The Effect of Nanometre-Scale Structure on Interfacial Energy. *Nat. Mater.* **2009**, *8*, 837–842.
11. Noguez, C. Surface Plasmons on Metal Nanoparticles: The Influence of Shape and Physical Environment. *J. Phys. Chem. C* **2007**, *111*, 3806–3819.
12. Chen, J.; Huang, Y.; Zhao, S.; Lu, X.; Tian, J. Gold Nanoparticles-Based Fluorescence Resonance Energy Transfer for Competitive Immunoassay of Biomolecules. *Analyst* **2012**, *137*, 5885–5890.
13. Zeng, S.; Yong, K.-T.; Roy, I.; Dinh, X.-Q.; Yu, X.; Luan, F. A Review on Functionalized Gold Nanoparticles for Biosensing Applications. *Plasmonics* **2011**, *6*, 491–506.
14. Saha, K.; Agasti, S. S.; Kim, C.; Li, X.; Rotello, V. M. Gold Nanoparticles in Chemical and Biological Sensing. *Chem. Rev.* **2012**, *112*, 2739–2779.
15. Liz-Marzán, L. M.; Murphy, C. J.; Wang, J. Nanoplasmonics. *Chem. Soc. Rev.* **2014**, *43*, 3820–3822.
16. Underwood, S.; Mulvaney, P. Effect of the Solution Refractive Index on the Color of Gold Colloids. *Langmuir* **1994**, *10*, 3427–3430.
17. Ross, M. B.; Ku, J. C.; Vaccarezza, V. M.; Schatz, G. C.; Mirkin, C. A. Nanoscale Form Dictates Mesoscale Function in Plasmonic DNA-Nanoparticle Superlattices. *Nat. Nanotechnol.* **2015**, *10*, 453–458.
18. Park, D. J.; Zhang, C.; Ku, J. C.; Zhou, Y.; Schatz, G. C.; Mirkin, C. A. Plasmonic Photonic Crystals Realized through DNA-Programmable Assembly. *Proc. Natl. Acad. Sci. U. S. A.* **2015**, *112*, 977–981.
19. Dadosh, T.; Gordin, Y.; Krahne, R.; Khivrich, I.; Mahalu, D.; Frydman, V.; Sperling, J.; Yacoby, A.; Bar-Joseph, I. Measurement of the Conductance of Single Conjugated Molecules. *Nature* **2005**, *436*, 677–680.
20. Peng, S.; McMahon, J. M.; Schatz, G. C.; Gray, S. K.; Sun, Y. Reversing the Size-Dependence of Surface Plasmon Resonances. *Proc. Natl. Acad. Sci. U. S. A.* **2010**, *107*, 14530–14534.
21. Myroshnychenko, V.; Rodríguez-Fernández, J.; Pastoriza-Santos, I.; Funston, A. M.; Novo, C.; Mulvaney, P.; Liz-Marzán, L. M.; García de Abajo, F. J. Modelling the Optical Response of Gold Nanoparticles. *Chem. Soc. Rev.* **2008**, *37*, 1792–1805.
22. Rodriguez-Lorenzo, L.; Alvarez-Puebla, R. A; de Abajo, F. J. G.; Liz-Marzan, L. M. Surface Enhanced Raman Scattering Using Star-Shaped Gold Colloidal Nanoparticles. *J. Phys. Chem. C* **2010**, *114*, 7336–7340.
23. Prodan, E.; Radloff, C.; Halas, N. J.; Nordlander, P. A Hybridization Model for the Plasmon Response of Complex Nanostructures. *Science* **2003**, *302*, 419–422.
24. Malola, S.; Lehtovaara, L.; Enkovaara, J.; Häkkinen, H. Birth of the Localized Surface Plasmon Resonance in Monolayer-Protected Gold Nanoclusters. *ACS Nano* **2013**, *7*, 10263–10270.
25. Zheng, N.; Fan, J.; Stucky, G. D. One-Step One-Phase Synthesis of Monodisperse Noble-Metallic Nanoparticles and Their Colloidal Crystals. *J. Am. Chem. Soc.* **2006**, *128*, 6550–6551.
26. Salzemann, C.; Zhai, W.; Goubet, N.; Pileni, M.-P. How to Tune the Au Internanocrystal Distance in Two-Dimensional Self-Ordered Superlattices. *J. Phys. Chem. Lett.* **2010**, *1*, 149–154.
27. Brust, M.; Walker, M.; Bethell, D.; Schiffrin, D. J.; Whyman, R. Synthesis of Thiol-Derivatised Gold Nanoparticles in a Two-Phase Liquid-Liquid System. *J. Chem. Soc., Chem. Commun.* **1994**, 801.
28. Templeton, A. C.; Hostetler, M. J.; Kraft, C. T.; Murray, R. W. Reactivity of Monolayer-Protected Gold Cluster Molecules: Steric Effects. *J. Am. Chem. Soc.* **1998**, *120*, 1906–1911.
29. Hostetler, M. J.; Templeton, A. C.; Murray, R. W.; Hill, C.; Carolina, N. Dynamics of Place-Exchange Reactions on Monolayer-Protected Gold Cluster Molecules. *Langmuir* **1999**, *15*, 3782–3789.
30. Jana, N. R.; Gearheart, L.; Murphy, C. J. Seeding Growth for Size Control of 5−40 nm Diameter Gold Nanoparticles. *Langmuir* **2001**, *17*, 6782–6786.
31. Bohren, C. F.; Huffman, D. R. *Absorption and Scattering of Light by Small Particles*; Wiley-VCH: Weinheim, 1983.
32. Wei, G.-T.; Yang, Z.; Lee, C.-Y.; Yang, H.-Y.; Wang, C. R. C. Aqueous-Organic Phase Transfer of Gold Nanoparticles and Gold Nanorods Using an Ionic Liquid. *J. Am. Chem. Soc.* **2004**, *126*, 5036–5037.
33. Link, S.; El-Sayed, M. A. Size and Temperature Dependence of the Plasmon Absorption of Colloidal Gold Nanoparticles. *J. Phys. Chem. B* **1999**, *103*, 4212–4217.

34. Moores, A.; Goettmann, F. The Plasmon Band in Noble Metal Nanoparticles: An Introduction to Theory and Applications. *New J. Chem.* **2006**, *30*, 1121.
35. Maier, S. A. *Plasmonics: Fundamentals and Applications*; Springer: New York, 2007.
36. Liz-Marzán, L. M.; Giersig, M.; Mulvaney, P. Synthesis of Nanosized Gold−Silica Core−Shell Particles. *Langmuir* **1996**, *12*, 4329–4335.
37. Samoc, A. Dispersion of Refractive Properties of Solvents: Chloroform, Toluene, Benzene, and Carbon Disulfide in Ultraviolet, Visible, and near-Infrared. *J. Appl. Phys.* **2003**, *94*, 6167–6174.
38. Johnson, P. B.; Christy, R. W. Optical Constants of the Noble Metals. *Phys. Rev. B* **1972**, *6*, 4370–4379.
39. Kreibig, U.; Vollmer, M. *Optical Properties of Metal Clusters*; Springer-Verlag: Berlin, 1995.
40. Hinterwirth, H.; Kappel, S.; Waitz, T.; Prohaska, T.; Lindner, W.; Lämmerhofer, M. Quantifying Thiol Ligand Density of Self-Assembled Monolayers on Gold Nanoparticles by Inductively Coupled Plasma-Mass Spectrometry. *ACS Nano* **2013**, *7*, 1129–1136.
41. Love, J. C.; Estroff, L. A; Kriebel, J. K.; Nuzzo, R. G.; Whitesides, G. M. Self-Assembled Monolayers of Thiolates on Metals as a Form of Nanotechnology. *Chem. Rev.* **2005**, *105*, 1103–1169.
42. Sabatani, E.; Cohen-Boulakia, J.; Bruening, M.; Rubinstein, I. Thioaromatic Monolayers on Gold: A New Family of Self-Assembling Monolayers. *Langmuir* **1993**, *9*, 2974–2981.
43. Palik, E. D. *Handbook of Optical Constants of Solids Dispersion Theory*; Palik, E. D., Ed.; Elsevier: New York, 1985; Vol. 1.
44. Etchegoin, P. G.; Le Ru, E. C.; Meyer, M. An Analytic Model for the Optical Properties of Gold. *J. Chem. Phys.* **2006**, *125*, 164705.
45. Lazzari, R.; Jupille, J.; Cavallotti, R.; Simonsen, I. Model-Free Unraveling of Supported Nanoparticles Plasmon Resonance Modes. *J. Phys. Chem. C* **2014**, *118*, 7032–7048.
46. Leng, J.; Opsal, J.; Chu, H.; Senko, M.; Aspnes, D. E. Analytic Representations of the Dielectric Functions of Materials for Device and Structural Modeling. *Thin Solid Films* **1998**, *313−314*, 132–136.
47. Hövel, H.; Fritz, S.; Hilger, A.; Kreibig, U. Width of Cluster Plasmon Resonances: Bulk Dielectric Functions and Chemical Interface Damping. *Phys. Rev. B: Condens. Matter Mater. Phys.* **1993**, *48*, 18178–18188.
48. Dufour, F.; Fresch, B.; Durupthy, O.; Chaneac, C.; Remacle, F. Ligand and Solvation Effects on the Structural and Electronic Properties of Small Gold Clusters. *J. Phys. Chem. C* **2014**, *118*, 4362–4376.